Core Heat Transport in the MAST Spherical Tokamak

A. R. Field, R. J. Akers, D. J. Applegate 1) , C. Brickley, P. G. Carolan, C. Challis, N. J. Conway, S. C. Cowley 1), G. Cunningham, N. Joiner 1), H. Meyer, A. Patel, C. Roach, M. Valovič, M. J. Walsh 2) and the MAST team

EURATOM/UKAEA Fusion Association, Culham Science Centre, Abingdon, Oxon, OX14 3DB, UK.

1) Imperial College, University of London, London, SW7 2BZ, UK.

2) Walsh Scientific Ltd., Culham Science Centre, Abingdon, Oxon, OX14 3EB, UK.

e-mail: anthony.field@ukaea.org.uk

Abstract High-β spherical tokamak (ST) plasmas have intrinsic properties which favour the suppression of anomalous transport. Transport has been studied in NBI heated plasmas in the MAST ST device, where it is found that ion thermal transport is typically close to the neo-classical level. Calculations of the ITG micro-stability with the GS2 gyro-kinetic code suggest that this form of turbulence may be suppressed by the high E×B shearing rates in these plasmas. Electron transport is somewhat higher and cannot be explained from mixing length estimates of ETG turbulence. This is perhaps due instead either to micro-tearing modes in the core plasma or extended radial structures in the saturated turbulence. Micro-stability is also favoured by low magnetic shear and this has been used to produce high-performance L- and H-mode plasmas with improved core confinement as well as plasmas exhibiting ITBs in both the ion and electron channels. Broad electron ITBs have been produced with counter-NBI heating in which anomalous electron transport apparently has been reduced by the very high E×B shearing rates prevailing in these plasmas. Such studies also contribute towards testing the transport and ITB physics basis for the ITER device.

1. Introduction

An understanding of transport processes in spherical tokamak (ST) plasmas is important for reliable prediction of the performance of future ST devices such as a Component Test Facility (CTF) [1] or a Spherical Tokamak Power Plant (STPP) [2]. First studies on the current generation of medium sized ST devices, MAST [3] and NSTX [4], are now permitting measurement of transport coefficients and their comparison with predictions for the anomalous transport based on gyro-kinetic simulations of the micro-stability using GS2 [5]. The results of these studies on MAST are summarised here together with results of experiments to form Internal Transport Barriers (ITBs) with co- and counter NBI heating.

The ST provides a unique environment for the study of core transport mechanisms in high-β, low aspect ratio plasmas, where it is predicted that anomalous transport might easily be suppressed to the underlying ion neo-classical level. A high pressure gradient, β', particularly in the presence of low magnetic shear, s, may reduce the growth rates, γ_m, of micro-instabilities, this reducing the drives due to the curvature and ∇B drifts, respectively [6]. The turbulence may then be de-correlated by the high intrinsic, pressure driven E×B flow shear ω_{SE} in the ST, where ω_{SE}/γ_m is expected to scale as ρ_i* [7]. The strong driven toroidal flow prevalent in current devices with tangential neutral beam injection (NBI) heating further enhances E×B flow shear thus favouring turbulence suppression.

As well as confirming the physics basis for future ST devices such studies challenge physics based models of anomalous transport [8] and ITB physics [9, 10] which are used to predict the performance of the ITER device and which underpin advanced operational scenarios.

2. Transport in L- and H-mode plasmas

The baseline operational scenario for ITER is the ELMy H-mode [11] and in the ST this also provides suitable T_e and n_e profiles and a confinement enhancement approaching that required

for the STPP ($H_{IPB(y,2)}$ ~ 1.6) [2]. Although the transient target heat loads due to the edge-localised-modes (ELMs) are predicted to be tolerable, alternative high-confinement scenarios where density and impurity control are achieved in the absence of ELMs would be preferable. Quasi-steady, sawteething, ELMy H-mode operation is achieved on MAST with merging-compression start-up, which results in an initially peaked current profile. Transport analysis of such a discharge is discussed in Section 2.1 below. Using an alternative start-up scenario, with an initial 0.1 MA from merging compression followed by a current ramp to produce a broad current profile, the onset of sawteeth can be delayed. This produces plasmas akin to those of 'hybrid' scenarios, which combine improved core confinement with an edge transport barrier (ETB) of H-mode plasmas. These discharges have a hollow current profile and central safety factor, $q_0 > 1$, as required for the STPP.

2.1 Quasi-steady state ELMy H-mode

The availability of state-of-the art imaging (visible bremsstrahlung for Z_{eff}) and kinetic profile diagnostics (ruby and NdYAG TS and CXRS systems) has allowed analyses of core transport in MAST using TRANSP [3, 12]. Such discharges have also been subject to study of their micro-stability using the gyro-kinetic code GS2 [13, 14]. In quasi-steady, H-mode discharge #6953 as presented in Ref. [3], at the half-radius region, $0.3 < \rho < 0.6$, where transport is not perturbed by sawteeth or ELMs, both the ion and electron heat diffusivities, $\chi_{i,e}$, are close to the ion neo-classical level, with $\chi_{i,e}$ ~ 1-3 χ_i^{NC}, or 2-5 m^2s^{-1}, while χ_e is significantly higher for ρ (~ r/a) > 0.6. This result is fairly robust to systematic uncertainties in the kinetic profile data, which can, however, strongly affect the derived transport coefficients in the outer regions of the plasma due to their influence on the ion-electron exchange term. In these NBI heated plasmas there is strong driven toroidal rotation, $V_{i\phi}$ ~ 100 km s^{-1}, corresponding to a toroidal Mach number, $M_\phi = V_{i\phi}/c_s$, where c_s is the sound speed, approaching 0.4. The contribution to the radial E-field, E_r, from the toroidal rotation dominates that due to the pressure gradient, resulting in a net positive plasma potential and a maximum ExB shearing rate ω_{SE} ~ 3×10^4 s^{-1} at ρ ~ 0.6. The current density profile, as predicted from poloidal field diffusion using TRANSP, is peaked resulting in a monotonic q profile with q_0 ~ 1. Results of micro-stability analysis of this discharge are summarised in Sect. 6 below.

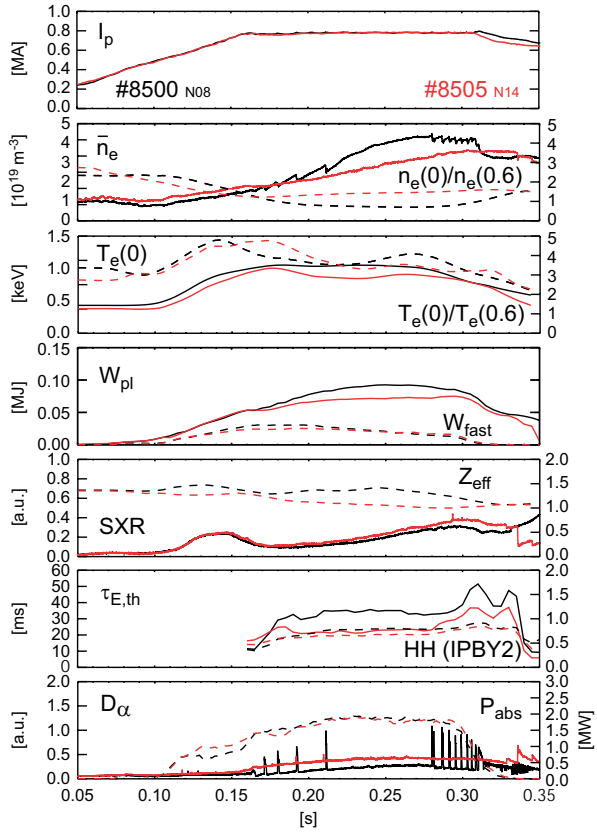

FIG. 1 Comparison of sawtooth-free H-(#8500) and L-mode (#8505) discharges showing evolution of I_p, $\bar{n}_e$, $T_e(0)$, n_e and T_e peaking factors, plasma energy, W_{pl}, fast-ion energy, W_{fast}, central Z_{eff} and SXR emission, thermal energy confinement time, $\tau_{E,th}$, H-mode quality factor H(IPB,y2), absorbed NBI power and divertor D_α emission. Dashed curves refer to right-hand axes.

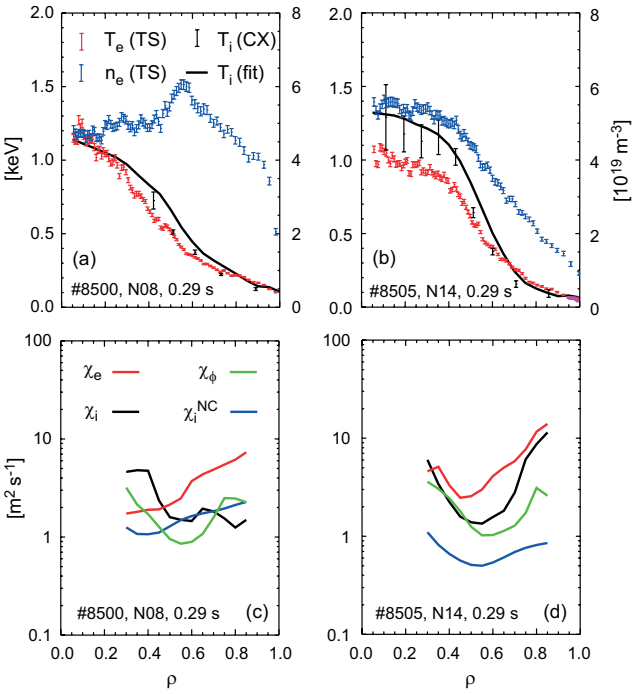

FIG. 2 Kinetic profiles (a, b) of sawtooth-free H- (#8500) and L-mode (#8505) discharges of FIG. 1 at 0.29 s with n_e and T_e from ruby TS system and T_i from CXRS on C^{6+} with extrapolated fit to T_i and results of TRANSP analysis of these discharges (c, d) showing electron and ion thermal diffusivities, $\chi_{i,e}$, momentum diffusivity, χ_ϕ, and Z-corrected neo-classical thermal diffusivity χ_i^{NC}.

2.2 Sawtooth-free L- and H-modes

The evolution of otherwise similar sawtooth-free, L- and H-mode discharges in MAST are shown in Fig. 1. These have a double-null-diverted (DND) configuration, high-field-side (HFS) gas puff fuelling and ~ 1.8 MW of NBI heating applied during the current ramp. The L-mode variant is produced by suppressing H-mode on shifting the plasma slightly downwards to produce an unbalanced DND configuration. The central electron temperatures, T_e (0) ~ 1-1.2 keV, and line-averaged densities, $\bar{n}_e \sim 4\times10^{19}$ m^{-3}, are similar at the time of NBI cut-off at 0.29 s when the T_i and $V_{i\phi}$ profiles are measured by CXRS.

The kinetic profiles measured at this time are shown in Fig. 2 (a, b). The onset of ELMs at 0.27 s reduces the edge density 'ears' of the ELM-free H-mode period allowing improved penetration of the CXRS measurement. The H-mode plasma has a more peaked T_e profile and broader n_e profile than the L-mode plasma with a steep edge density gradient due to the H-mode ETB and the central n_e profile is hollow. The L-mode plasma has a higher central T_i ~ 1.3 keV with a steep gradient region between ρ ~ 0.4-0.6. In the H-mode discharge the stored energy, W_{pl} ~ 95 kJ, is about 20% higher than in the L-mode discharge with the fast ion fraction, W_{fast}/W_{pl}, decreasing with increasing density to ~ 20% later in the discharge. The central Z_{eff} remains below 1.5 and the SXR emission shows no sign of impurity accumulation or sawteeth. The thermal energy confinement time, $\tau_{E,th}$ ~ 35 ms, of the H-mode plasma is a factor ~ 1.4 higher than in L-mode which has $\tau_{E,th}$ ~ 24 ms [15].

Time-dependent TRANSP analysis of these discharges is performed using the profiles of Figs. 2 (a, b), together with the T_e and n_e profile evolution from the NdYAG TS system. The T_i and $V_{i\phi}$ evolution is approximated by assuming constant radial profiles of T_i/T_e and M_ϕ. The resulting transport coefficients are shown in Figs. 2 (c, d). In the H-mode plasma χ_i (~ 1-2 m^{2}s^{-1}) is at or below χ_i^{NC} outside ρ ~ 0.5. These χ_i values are about 0.01 χ_{GB} ($\chi_{GB} = c_s\rho_s^2/L_n$) in the half radius region and 0.1 χ_{GB} at the periphery of the plasma. The momentum diffusivity, χ_ϕ, decreases to about a factor 2 below χ_i at ρ ~ 0.6. In contrast, the electron thermal diffusivity, $\chi_e > \chi_i$, increasing with radius from ~ 2 to 4 times χ_i^{NC}.

In the L-mode plasma the transport coefficients $\chi_{i,e}$ in the core, $\rho < 0.6$, are very similar to those in the H-mode plasma. However, both χ_i and χ_e increase strongly in the plasma periphery. The normalised pressure gradient $\beta' = d\beta/d\rho$ peaks at 0.4 and 0.8 in the L- and H-mode plasmas respectively at $\rho \sim 0.6$.

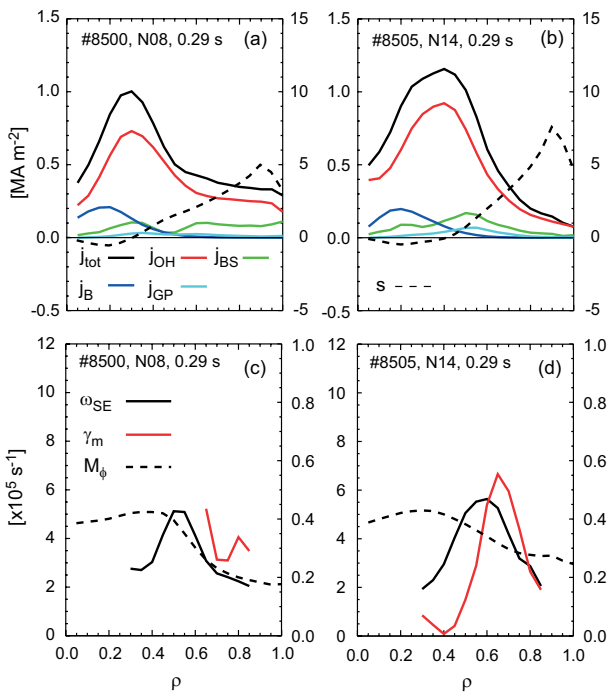

FIG. 3 Results from TRANSP analysis of the discharges of FIG 1 at 0.29 s, showing: (a, b) contributions from ohmic, j_{OH}, bootstrap, j_{BS}, beam-, j_B, and pressure-driven, j_{GP}, components to the total current density j_{tot} and magnetic shear s and (c, d) the E×B shearing rate, ω_{SE}, compared to the maximum ITG growth rate, γ_m, and the toroidal Mach number, M_ϕ. The dashed curves refer to the right-hand axes.

Current density profiles predicted from TRANSP poloidal field diffusion calculations are shown in Figs. 3 (a, b). These are hollow in both L- and H-mode, with a minimum in the magnetic shear, $s = (r/q)\,dq/dr$, at $\rho \sim$ 0.3-0.4 and $q_{min} > 1$. Both the ohmic and bootstrap current density profiles are broader in H-mode due to the broader n_e and pressure profiles. The NBI power and torque deposition profiles are peaked in both discharges with similar NBI driven current.

In both discharges the toroidal Mach number, $M_\phi \sim 0.4$ in the core, decreasing to ~ 0.2 in the periphery. The corresponding ExB flow shear: $\omega_{SE} \cong \left| RB_\theta / B_\phi \partial (E_r / RB_\theta) / \partial r \right|$, [16] is dominated by the contribution to the radial E-field, $E_r = \nabla p_i / eZ_i n_i + V_{i\phi} B_\theta - V_{i\theta} B_\phi$, from the driven toroidal flow, $V_{i\phi} B_\theta$. This peaks at about $\omega_{SE} \sim 5\times10^5$ s^{-1} at $\rho \sim$ 0.5-0.6 where the transport coefficients are lowest relative to gyro-Bohm levels. In this region, in the L-mode plasma ω_{SE} exceeds the estimated growth rate, γ_m, for ion-temperature-gradient (ITG) modes which may thus be stabilized (see Sect. 4 below). In the peripheral region, however, the ExB shear may not be sufficient to stabilize this form of turbulence. (Recent calculations of ITG stability with GS2 for the L-mode discharge considered here for a single flux surface ($\rho = 0.6$) are broadly consistent with the analytic estimates for γ_m presented here.) Note that the hollow n_e profile in the core of the H-mode plasma results in a negative value of η_i (= L_n/L_T) in which case the form used below for γ_m is invalid. As discussed in Sect. 6, calculations with GS2 show that γ_m for ITG modes can increase strongly for $\eta_i < 0$.

3. ITB formation with co- and counter-NBI

Observations of internal transport barriers (ITBs) in MAST readily test accepted ITB existence criteria [17] and help to validate micro-stability calculations. ITBs are formed in MAST by early NBI heating of low density plasmas during a current ramp to produce weak or reversed magnetic shear and strong driven toroidal rotation, $V_{i\phi} \sim 250$ km s^{-1} [18]. Marked differences in the ITB character between similar discharges with co- and counter-NBI heating highlight the profound influence that changes to the ExB shearing rate and the magnetic shear can have on anomalous transport [19, 20, 21].

A comparison of $T_{i,e}$ and n_e profiles from otherwise similar ITB discharges with co- and counter-NBI heating is shown in Fig. 4, together with the associated thermal, $\chi_{i,e}$, and

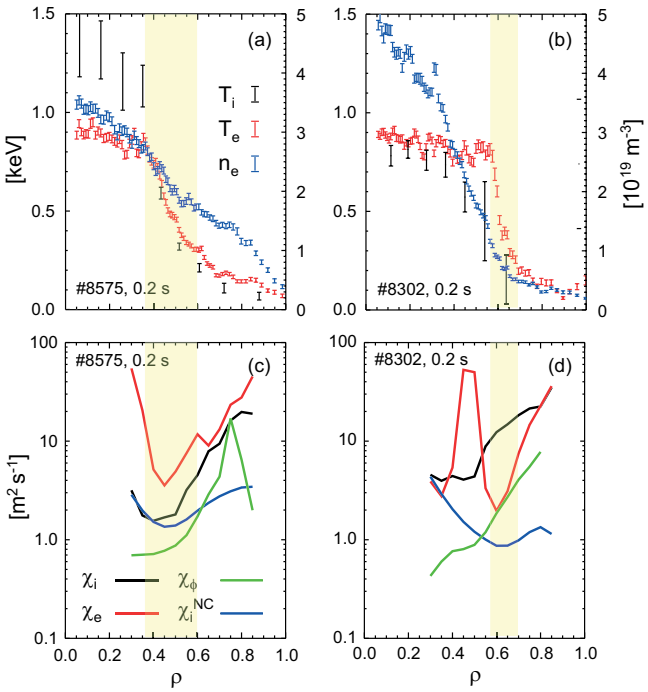

FIG. 4 Kinetic profiles (a, b) and results of TRANSP analysis (c, d) of ITB discharges with co- (#8575) and counter (#8302) NBI heating at 0.2 s.

momentum, χ_ϕ, transport coefficients. The neo-classical ion thermal diffusivity, χ_i^{NC} (Z-corrected Chang-Hinton [22]) is also shown.

With co-NBI an ion ITB is produced with $R/L_T \sim 15$ and $\chi_i \sim \chi_i^{NC}$ at $\rho \sim 0.5$, which is close to the location where $s \sim 0$ as shown in Fig. 5. There is a weaker suppression of electron thermal transport in this region where $R/L_T \sim 10$ and $\chi_e \sim$ 2-3 χ_i^{NC}. The current density profile is hollow as shown in Fig. 5, primarily due to an off-axis peaking of the ohmic current density. There is significant on-axis neutral beam driven and bootstrap contribution to the total current density. The radial E-field, E_r, is predominantly due to the driven toroidal flow, $V_{i\phi}$, with the pressure gradient contribution reducing the net positive plasma potential. The corresponding E×B flow shear, ω_{SE}, is shown, which exhibits a maximum in the ITB region of $\omega_{SE} \sim 6\times10^5$ s^{-1}. This is compared to an analytic prediction for the ITG growth rate, γ_m, as discussed below.

With counter-NBI the dominant contribution to E_r from the driven toroidal flow, $V_\phi B_\theta$, results in a negative plasma potential and is augmented by the pressure gradient, resulting in higher values of $\omega_{SE} \sim 10^6$ s^{-1} at larger radius, $\rho \sim 0.6$. Under these conditions a strong electron ITB with $R/L_{Te} \sim 20$ is produced at a broader radius, with $\chi_e \sim 2\,\chi_i^{NC}$ at $\rho \sim 0.6$. The on-axis, counter-NBCD helps to broaden the low-s region compared to the co-NBI case. Remarkably, at the location of the eITB the ion thermal transport is high with $\chi_i \sim 10\,\chi_i^{NC}$. A reduction of high frequency (0.2-0.5 MHz) density turbulence in the vicinity of the eITB is also observed by means of reflectometry [19].

4. Shear-flow stabilisation

Reduction of anomalous transport should occur when the de-correlation due to the E×B shear exceeds the growth rate of the most unstable mode, $\omega_{SE} > \gamma_m$ [23]. An appropriate estimate of the ITG growth rate for conditions of low magnetic shear, $|L_s/L_n| >> 1$, where there is negligible overlap between modes on neighbouring resonant surfaces (where $m - nq = 0$) is given by:

$$\gamma_m^{ITG} = (\eta_i - 2/3)^{3/4} |s|^{1/2} c_i / |L_s| \qquad (1)$$

where $\eta_i = L_n/L_T$, $c_i = (T_i/M_i)^{1/2}$ and $L_s = qR/s$ [24]. This form of γ_m^{ITG} is appropriate for conditions where toroidicity enhances the role of the parallel ion dynamics and resonant wave-particle interactions. In the co-NBI case shown in Fig. 5 $\omega_{SE} > \gamma_m^{ITG}$ in the vicinity of

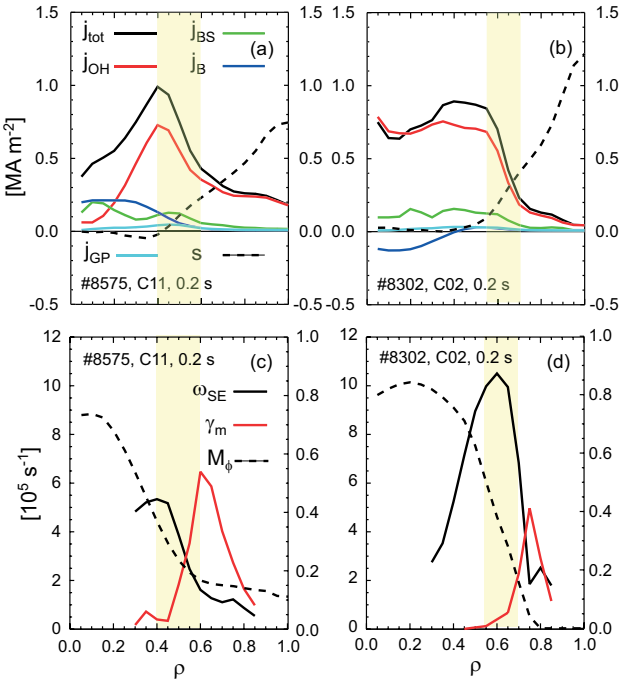

FIG. 5 Results from TRANSP analysis of the discharges of FIG 4 at 0.2 s, showing: (a, b) current density profiles; and (c, d) the E×B shearing rate ω_{SE} compared to the maximum ITG growth rate γ_m and the toroidal Mach number, M_ϕ.

the ion ITB, which is consistent with the suppression of transport due to ITG turbulence in this region, where the criterion $|L_s/L_n| >> 1$ is also satisfied. Although the ExB shearing rate is higher in the counter-NBI discharge, with $\omega_{SE} >> \gamma_m^{ITG}$, in the vicinity of the eITB, the ion transport is high in this region, while the electron transport is strongly reduced instead, which is a remarkable observation. Note that the MHD activity with counter-NBI is very different in character to that with co-NBI [18].

5. ITB formation criteria

MAST data have contributed to a multi-machine analysis of ITB existence criteria [17], where it was found that criteria such as those on R/L_T or ρ_T*, where $\rho_T^* = \rho_s/L_T$ and ρ_s is the ion Larmor radius at the sound speed, are not generally applicable. The criterion $\rho_T^* > \rho_{ITB}^* \sim 0.014$ was found to be a reliable indication of ITB existence over a wide variety of JET discharges [25]. It is justified from scaling arguments using a generic form for the growth rate of drift instabilities, $\gamma_m = (c_s / L_T)\, G_1(s, \beta, T_e/T_i, \nu^*, \ldots)$, where G_1 is a function of order unity [26], and by assuming that the temperature gradient provides the dominant contribution to the ExB flow shear, resulting in the scaling $\omega_{SE} \sim (c_s / L_T)\, \rho_T^*$. Under conditions on MAST with strong, unbalanced tangential NBI heating, where the toroidal Mach number M_ϕ can approach unity, the driven toroidal flow dominates the ExB flow shear and this criterion is not appropriate. Indeed, it is found that $\rho_T^*/\rho_{ITB}^* \sim 10$ even in standard MAST L-mode discharges. An alternative criterion can be derived under the assumption that the toroidal flow dominates the ExB flow shear. This results in the scaling $\omega_{SE} \sim (B_\theta / B_\phi)(c_s / L_T)$ suggesting that a critical Mach number, $M_\phi^{ITB}(s, \beta, L_T, T_e/T_i, \nu^*, \ldots)$, is required for ITB formation. This was pointed out in an earlier study of the effect of toroidal rotation on confinement in TFTR [27].

6. Micro-stability studies

Work is progressing towards a first-principles physics based understanding of the transport processes in the ST using the gyro-kinetic code GS2 [5]. Linear stability calculations have been performed for a typical MAST ELMy H-mode discharge (#6252) for ITG ($k_\perp\rho_i$ < O(1)) and electron-temperature gradient (ETG) modes ($k_\perp\rho_i$ > O(1)) [13, 28]. These show that electromagnetic effects destabilise micro-tearing modes with $k_\perp\rho_i$ < O(1) and stabilise ETG modes. In the core plasma at $\rho \sim 0.4$, the eigenmodes are highly extended along the field lines with tearing parity (even in $A_{||}$) and have the character of micro-tearing modes. Growth rates for the ITG branch also increase dramatically for $\eta_i < 0$, e.g. with hollow density profiles as in

the H-mode plasma in Fig. 2a. At larger radius the electromagnetic ITG modes do not have tearing parity and the growth rates increase with radius, resulting in a mixing length estimate for the transport due to these modes of χ_{ITG} ($\sim \gamma_m/k_\perp^2$) ~ 3.3 m^2s^{-1} at $\rho \sim 0.6$, close to the observed χ_i value. It is estimated, however, that the pressure driven E×B shearing rate would significantly stabilise these modes.

ETG modes are found to be less extended along the field lines and are stabilised by electromagnetic effects. Growth rates for these modes are much higher than for ITG modes with $\gamma_m \sim 1.3\times10^6$ s^{-1} for $k_\perp\rho_i \sim 25$ at $\rho \sim 0.6$ resulting in a mixing length estimate for $\chi_{ETG} \sim$ 0.085 m^2s^{-1} which is much too small (due to the high $k_\perp$ of these modes) to account for the electron transport. Fully non-linear calculations are necessary to predict the saturated turbulence spectrum and the corresponding transport. First such calculations of ETG turbulence have been performed for MAST [29], where it is found that finite β effects may be significant on the inner surfaces. Large amplitude, radially extended streamer structures are found to be very weakly damped by zonal flows, and these structures generate substantial cross-field transport with $\chi_e^{ETG} \sim 10$ m^2s^{-1}, which is somewhat above the observed values.

Micro-stability calculations for NSTX-like ST equilibria made using the GS2 code show that growth rates for ITG and ETG modes, although initially increasing with β', are reduced when $\beta' > 2$ [6]. In the MAST discharges discussed here, the prevailing values of $\beta' \sim$ 0.3-0.8 are well below the threshold predicted for the onset of β' stabilisation. Recent analytical studies of micro-stability in the presence of a minimum in q show that low magnetic shear can have a profound effect on the mode structure of trapped electron (TEM) and ITG modes [30], where radially extended modes are replaced by narrow modes at the resonant surfaces which would be less effective in generating transport. A further prediction is that collisions may fully stabilise TEM modes in the presence of a steep density barrier where $\varepsilon_n = L_n/R << 1$. In both of the ITB discharges in Fig. 4 (and to a lesser extent the L-mode discharge of Fig. 2) there is a local steepening of the density profile in the vicinity of the ITB which would thus favour TEM stability.

7. Summary & Conclusions

Transport coefficients have been measured in NBI heated L- and H-mode plasmas in the MAST ST device. At the half-radius region, ion thermal diffusivities are close to the ion neo-classical level. The strong toroidal flow driven by the tangential NBI heating of these plasmas, resulting in toroidal Mach numbers of order unity produces the dominant contribution to the radial E-field in the plasmas. Estimates of maximum growth rates of ITG micro-instabilities, both from analytic theory and from gyro-kinetic micro-stability calculations, indicate that the prevailing, NBI driven E×B shearing rates are sufficient to reduce this form of turbulent transport. Mixing length estimates of thermal diffusivity χ_{ITG} due to the dominant ITG modes are close to the observed levels of transport.

Electron thermal diffusivities are observed to be typically somewhat higher than χ_i in MAST L- and H-mode plasmas. Growth rates for ETG micro-instabilities in H-mode plasmas determined using GS2 are typically too high to be stabilised by the usual level of E×B flow shear. However, mixing length estimates of χ_{ETG} are too small to account for the observed level of transport but non-linear calculations suggest significant transport from streamers. In the core plasma micro-tearing modes, which are destabilised by low magnetic shear, are found in ITG stability calculations with GS2, which may enhance electron thermal transport along stochastic field lines.

Plasmas with low or reversed magnetic shear can be produced by heating during the initial current ramp resulting in a hollow current profile. The sawtooth free L- and H-mode plasmas

produced in this way exhibit reduced core transport perhaps due to the improved ITG micro-stability, which is favoured by low magnetic shear. Extreme examples are the ITB discharges produced with early NBI heating of low density target plasmas, the co-NBI discharge exhibiting an ITB in both the ion and electron channels at the half-radius region. The high E×B flow shear produced in the counter-NBI case results in a strong electron ITB at broad radius where the ETG turbulence is apparently suppressed. The presence of a minimum in q in the ITB region is also predicted to favour ITG and TEM stability, particularly in the presence of a steep density gradient.

Rapid progress has been made in the understanding of, and ability to manipulate, the anomalous transport in ST plasmas, which have inherent properties that favour turbulence stabilisation. It remains to be determined whether sustained advanced operational scenarios suitable for an STPP or CTF device can be developed with upgrades to current ST devices.

References

[1] H. R. Wilson, G. M. Voss, R. J. Akers et al., UKAEA Culham, PPN 2004/5.1.
[2] H. R. Wilson, J. W. Ahn, R. J. Akers et al., Nucl. Fusion, **44** (2004) 917-929.
[3] R. J. Akers, J. W. Ahn, G. Y. Antar et al., Plasma Phys. Contr. Fusion, **45** 12A (2003) A175-204.
[4] B. P. LeBlanc, R. E. Bell, S. M. Kaye et al., Nucl. Fusion, **44** (2004) 513-523.
[5] M. Kotchenreuther, G. Rewoldt, W. M. Tang, Comput. Phys. Commun. **88** (1995) 128.
[6] C. Bourdelle, W. Dorland, X. Garbet et al., Phys. Plasmas, **10** 7 (2003) 2881.
[7] M. Kotchenreuther, W. Dorland, Q. P. Liu et al., Nuclear Fus., **40** 3Y (2000) 677.
[8] J. W. Connor. H. R. Wilson, Plasma Phys. Contr. Fusion, **36** (1994) 719-795.
[9] J. W. Connor, T. Fukuda, X. Garbet et al., Nucl. Fusion, **44** (2004) R1-R49.
[10] P. Gohil, J. Kinsey, V. Parail et al., Nucl. Fusion **43** 8 (2003) 708-715.
[11] ITER Physics Basis Editors, Nucl. Fusion, **39** (1999) 2137-2174.
[12] A. Pankin, D. McCune, R. Andre et al., Computer Phys. Comm., **159** 3 (2004) 157-184.
[13] C. M. Roach, D. J. Applegate, J. W. Connor, et al., Proceedings of 31st EPS Conf. on Contr. Fusion and Plasma Phys., ECA Vol. 28G, P4-190, London, 2004.
[14] D. J. Applegate, C. M. Roach, S. C. Cowley et al., accepted for publication in Phys. of Plasmas, 2004.
[15] M. Valovic, H. Meyer, R. J. Akers, paper EX/P6-30, this conference.
[16] R. V. Budny, B. Alper, D. N. Borba et al., Nucl. Fusion **42** 1 (2002) 66-75.
[17] T. Fujita, T. Aniel, E. Barbato et al. Proceedings of 30th EPS Conf. on Contr. Fusion and Plasma Phys., Vol. 27A, P2-131, St. Petersburg, 2003.
[18] A. R. Field, R. J. Akers, N. J. Conway, Proceedings of 30th EPS Conf. on Contr. Fusion and Plasma Phys., Vol. 27A, P3-93, St. Petersburg, 2003.
[19] A. R. Field, R. J. Akers, C. Brickley et al., Proceedings of 31st EPS Conf. on Contr. Fusion and Plasma Phys., Vol. 28G, P4-187, London, 2004.
[20] H. Meyer, A. R. Field, R. J. Akers et al., Plasma Plasma Phys. Contr. Fus., **46** 5A (2004) A291-A298.
[21] R. J. Akers and the MAST team, paper EX/4-4, this conference.
[22] C. S. Chang, F. L. Hinton, Phys. Fluids, **29** (1986) 3314.
[23] T. S. Hahm, K. H. Burrell, Phys. Plasmas, **2** 5 (1995) 1684-1651.
[24] A. L. Rogister, Nucl. Fusion, **41** 8 (2001) 1101-1106.
[25] G. Tresset, X. Litaudon, D. Moreau, X. Garbet, Nucl. Fusion, **42** 5 (2002) 520-526.
[26] J. W. Connor, J. B. Taylor, Proc. 10th IAEA London, 1984, Vol. II (IAEA Vienna), p. 13.
[27] S. H. Batha, S. D. Scott, D. R. Mikkelsen, Proceedings of 24th EPS Conf. on Contr. Fusion and Plasma Phys., Berchtesgaden, ECA, Vol. 21A, Part III, 1997.
[28] C. M. Roach, D. J. Applegate, S. C. Cowley et al., "Theory of Fusion Plasmas", Proceedings of Joint Varenna-Lausanne International Workshop, Varenna, 2004.
[29] N. Joiner, D. Applegate, S. C. Cowley, Proceedings of 31st EPS Conf. on Contr. Fusion and Plasma Phys., Vol. ECA 28G, P4-189, London, 2004.
[30] J. W. Connor, R. J. Hastie, Plasma Phys. Contr. Fusion, **46** (2004) 1501-1535.

Acknowledgements

This work is funded jointly by the UK Engineering and Physical Sciences Research Council and EURATOM.